34th Annual International Conference of the IEEE EMBS
San Diego, California USA, 28 August - 1 September, 2012

Locating the STN-DBS electrodes and resolving their subsequent networks using coherent source analysis on EEG

Muthuraman M, Paschen S, Hellriegel H, Groppa S, Deuschl G, Raethjen J

Abstract— **The deep brain stimulation (DBS) of the subthalamic nucleus (STN) is the most effective surgical therapy for Parkinson's disease (PD). The first aim of the study was to locate the STN-DBS electrode by applying source analysis on EEG. Secondly, to identify tremor related areas which are associated with the STN. The Dynamic imaging of coherent sources (DICS) was used to find the coherent sources in the brain. The capability of the source analysis to detect deep sources like STN in the brain using EEG data was tested with two model dipole simulations. The simulations were concentrated on two aspects, the angle of the dipole orientation and the disturbance of the cortical areas on locating sub-cortical regions. In all the DBS treated Parkinsonian tremor patients the power spectrum showed a clear peak at the stimulated frequency and followed by there harmonics. The DBS stimulated frequency constituted a network of primary sensory motor cortex, supplementary motor area, prefrontal cortex, diencephalon, cerebellum and brainstem. Thus the STN was located in the region of the diencephalon. The resolved network may give better understanding to the pathophysiology of the effected tremor network in PD patients with STN-DBS.**

I. Introduction

The subthalamic nucleus (STN) is currently most common target and stimulation of this structure is particularly very successful in reducing tremor [1-3]. Firstly, the most reliable tool used to locate the electrode has been the MRI [4, 5]. However, the image distortion caused by the local magnetic field in homogeneity of electrodes could be a concern for the accuracy of the MR images in estimation of the electrode position [6]. Inorder to avoid this, recently there have been other tools used in combination like CT and MRI to locate the electrodes [7]. Secondly, the network connected to the STN is well studied in both rodents and primates [8]. In humans there have been few studies using diffusion tensor imaging (DTI) [9] studying the cortical and sub-cortical connections of human STN [10]. Inorder to solve both these questions we use dynamic imaging of coherent sources (DICS) which uses a beamforming approach to identify the voxel with the highest power in the brain for a specific frequency band [11]. Later, this voxel can be used as noise for the subsequent run to find coherent networks involved in the brain [12]. The two constraints tested in this study with two simulations are the dependency on the angle of the dipole orientation, the disturbance of the cortical areas for locating sources in the sub-cortical regions. Both the simulations were done to test the capability of this method in robustly locating sources in the sub-cortical regions of the brain. The sources for the DBS stimulated frequency and there corresponding network components were estimated in all the Parkinsonian patients.

*Research supported by SFB 855 Project D2.

M. Muthuraman., is with the Department of Neurology, Christian Albrechts university Kiel, 24105 Germany (phone: 0049-431-597-8804; fax: 0049-431-597-8502; e-mail: m.muthuraman@neurologie.uni-kiel.de).

S. Paschen., is with the Department of Neurology, Christian Albrechts university Kiel, 24105 Germany (e-mail: s.paschen@neurologie.uni-kiel.de).

H. Hellriegel., is with the Department of Neurology, Christian Albrechts university Kiel, 24105 Germany (e-mail: h.hellriegel@neurologie.uni-kiel.de).

S. Groppa., is with the Department of Neurology, Christian Albrechts university Kiel, 24105 Germany (e-mail: s.groppa@neurologie.uni-kiel.de).

G. Deuschl., is with the Department of Neurology, Christian Albrechts university Kiel, 24105 Germany (e-mail: g.deuschl@neurologie.uni-kiel.de).

J. Raethjen., is with the Department of Neurology, Christian Albrechts university Kiel, 24105 Germany (e-mail: j.raethjen@neurologie.uni-kiel.de).

II. Methods

A. Power Spectrum

The power spectrum is estimated using the multitaper method [13]. Let $y(t)$ be the signal, and then the power spectrum can be defined as:

$$P_{MT}(q) = \frac{1}{T}\sum_{i=1}^{T}\left|\widetilde{Y}_i(q)\right|^2 \qquad (1)$$

where $\widetilde{Y}_i(q)$ is the Fourier transform of the windowed signal $y(t)$ which can be estimated as:

$$\widetilde{Y}_i(q) = \sum_{t=1}^{M} d_t(i)\, y(t) \exp(-2\pi fqt) \qquad (2)$$

here $d_t(i)(i = 1,2,\cdots T)$ are the T orthogonal tapers. The discrete prolate spheroidal sequences (DPSS) are chosen as the orthogonal windows due to there good leakage and spectral properties [14].

B. Forward Model

The forward problem is the computation of the scalp potentials for a set of neural current sources. It is usually solved by estimating the so-called lead-field matrix [15] with specified models for the brain. In this study, the more complex five-concentric-spheres model (see Fig. 1) was used to create the volume conductor model with standard T1 magnetic resonance images [16].

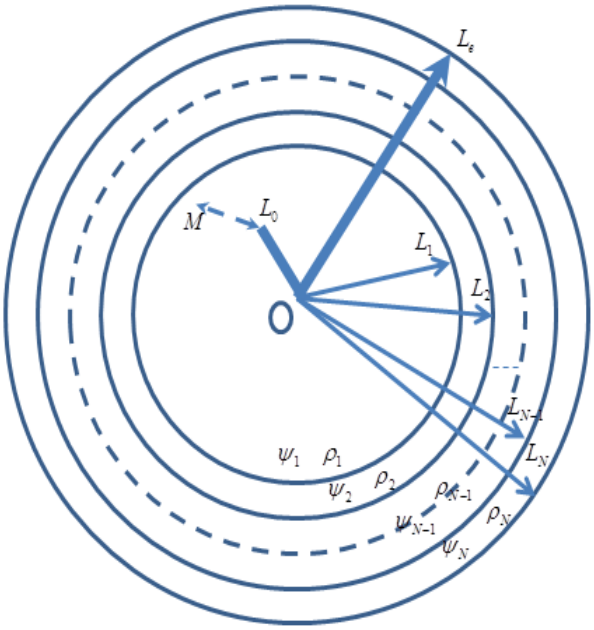

Figure 1. The notations used in describing a dipole within an N-layer anisotropic sphere. The outermost layer radius of the sphere is L_N. The potential at $L_e(L_e = L_N)$ due to a dipole located at L_0 within the innermost layer with moment M is computed.

Let the layer radius, layer radial conductivities, and layer tangential conductivities of an N-layer concentric anisotropic sphere be L_s, ρ_s, and ψ_s $(L_s > L_{s-1}; s = 1,2,\cdots,N)$, respectively. The anisotropic here means that, in each layer, the radial conductivity may be different from the tangential conductivity, but both conductivities are constants. A dipole with moment M is located at L_0 within the innermost layer, $|L_0| = L_0 < L_1$. Then, using a derivation similar to those described in [17, 18], the observed potential on the N - Layer sphere surface at $L_e(|L_e| = L_e = L_N)$ is

$$Q^A(L_0, M; L_e) = \frac{M}{4\pi\rho_N L_e^2}\sum_{n=1}^{\infty}\frac{2n+1}{n}\left(\frac{L_0}{L_e}\right)^{n-1}$$

$$\times\left[a_n n\cos\alpha\, P_n(\cos\gamma) + b_n \cos\beta \sin\alpha\, P_n^1(\cos\gamma)\right] \quad (3)$$

α is the angle between dipole location L_0 and the dipole moment M. γ is the angle between L_0 and the observation L_e. L_0 and M define a plane $P1$; L_0 and L_e define a another plane $P2$; β is the angle between $P1$ and $P2$. P_n and P_n^1 are the Legendre polynomials, respectively.

$$a_n = \frac{\nu_1}{n} b_n; \text{ where} \quad (4)$$

$$\nu_1 = \left[\sqrt{1+4n(n+1)\psi_i}/\rho_i - 1\right]/2; (i = 1,2,..,N) \quad (5)$$

$$\begin{bmatrix} m_{11} & m_{12} \\ m_{21} & m_{22} \end{bmatrix} = \prod_{k=1}^{N-1}\frac{1}{2\nu_k + 1}\begin{bmatrix} R_{11} & R_{12} \\ R_{21} & R_{22} \end{bmatrix} \quad (6)$$

The matrices in the above equation are non-commuting and the matrix with the highest index is to be first applied. If $N = 1$, the product of (6) needs to be replaced by an identity matrix. To be noted that $L_e = L_N$ in equation (3-6). Q^A can be broken down into two parts: $Q_r^A(L_0, M_r; R_e)$, the part due to the radial component (the terms containing P_n), and $Q_t^A(L_0, M_t; R_e)$, the part due to the tangential component (the terms containing P_n^1), where $M_t = M\cos\alpha$ and $M_t = M\sin\alpha$ are the radial and tangential dipole moments, respectively. If we consider the innermost layer is anisotropic, then $\nu_1 \neq n$. The a_n and b_n are functions of the dipole parameter, L_0. Since, a_n and b_n depend only on L_0 and not on other dipole parameters or electrode locations. The computation can be simplified by computing the L_0 dependent Berg parameters at each L_0. Because $\nu_1 \neq n$, $a_n \neq b_n$, the radial and the tangential parts need to be fitted separately. The a_n and b_n can be expressed in the following way for all n:

$$a_n = \sum_{j=1}^{J_T}\lambda_j(L_0)\,\mu_j^{n-1}(L_0)$$
$$b_n = \sum_{j=1}^{J_t}\tau_j(L_0)\,\eta_j^{n-1}(L_0) \quad (7)$$

where the λ, μ, τ, η are proper L_0 dependent Berg parameters. J_T and J_t are the numbers of Berg dipoles for a radial dipole and a tangential dipole, respectively. Then, equation (3) can be written as:

$$Q^A(L_0, M; L_e) = \sum_{j=1}^{J_T} Q_T^H\left(\mu_j(L_0)L_0, \lambda_j(L_0)M_T; L_e\right) +$$
$$\sum_{j=1}^{J_t} Q_t^H\left(\eta_j(L_0)L_0, \tau_j(L_0)M_t; L_e\right) \quad (8)$$

Equation (8) states that the surface potential generated by one radial dipole, with magnitude M_T located at L_0 within an anisotropic multilayer sphere is equal to the surface potential generated by J_T radial dipoles, with magnitudes

$\lambda_j(L_0)M_T$, located at $\mu_j(L_0)L_0\ (j=1,2\ldots,J_T)$, within a one-layer homogeneous sphere while assuming the one-layer and the N-layer spheres is equal to the radial conductivity of the outermost layer of the N-layer sphere. The same holds true for the tangential dipole. Because the terms of Q^A decrease with increasing n due to the factor $(L_0/L_e)^{n-1}$, in order to fit the λ, μ, τ, η parameters, the quantities Δ_T and Δ_t should be minimized at each L_0. If we consider that the first term of a_n and b_n should be fitted completely,

$$a_n = \sum_{j=1}^{J_T} \lambda_j(L_0) \text{ and } b_n = \sum_{j=1}^{J_t} \eta_j(L_0) \quad (9)$$

then the equation (9) can be extended so that the Berg parameters λ, μ, τ, η should be fitted at distance $L_0\ (0 \le L_0 < L_1)$. Since the parameters have to fitted under each L_0 in extended equation (9) the L_0 should not be replaced by L_1. Also the terms J_T and J_t may be different for a certain accuracy. The complete description of the forward solution is described elsewhere [19]. The inverse solution, the power and coherence estimated using the Multitaper method (MTM) as described in section A, at any given location in the brain can be computed using a linear transformation which in our case is the spatial filter. The spatial filter relates the electromagnetic field on the surface to the underlying neural activity in a certain brain region. The neural activity is modeled as a current dipole or sum of current dipoles. The spatial filter is described in [20], which attenuates the signals from other locations and allows only signals generated from a particular location in the brain.

III. Model Simulation

In the **first simulation**, the data is generated by assuming an autoregressive process of order two, and taking $\varepsilon(t)$ as the driving white Gaussian noise with unit variance. The source for the 90 Hz was implemented in one voxel in the STN at voxel number 560 in the left-side and producing the EEG signal with a broad-band AR2 plus white noise of 25% (SNR=4dB) (compared to the clean 90 Hz AR2 signal of infinite SNR) was added to the other voxels. The dipole orientations α are changed from 0° to 180° in steps of 10° to see whether the source analysis is capable of identifying the dipole orientations with a 64-channel EEG arrangement assumed for the forward model. Due to clarity, the simulation results shown in Fig. 2 B are only for the dipole orientations results at 0°, 60°, 120° and 180°. But, all the dipole orientations were identified correctly by the method with these model parameters in simulating a dipole in the STN.

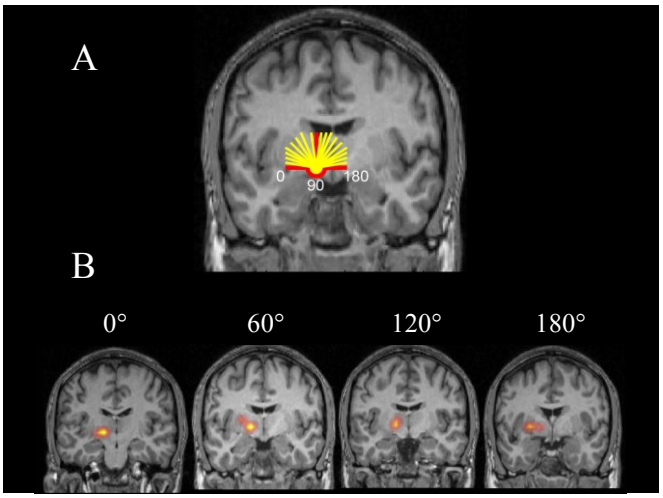

Figure 2. A. The simulated dipole angle orientations from 0° to 180° in steps of 10° shown by the yellow lines. B. For clarity only the results for 0°, 60°, 120° and 180 are shown.

In the **second simulation**, the recorded EEG data from a patient was used to test the disturbances of the cortical areas on locating sources in the sub-cortical regions. In this patient only the left-side contact 9- and G+ unipolar stimulation was done with 90 Hz, 450 microseconds, at 1.2 V. The first run of the source analysis was applied on the recorded EEG data and the results are shown in Fig.3 B. But, for the second run we considered the cortical area voxels marked in yellow in Fig. 3 A as noise and estimate the sources in the sub-cortical regions and the results are shown in Fig. 3 C. The results were improved by not considering the cortical voxels and the estimated source was deeper compared to first run of the simulation results.

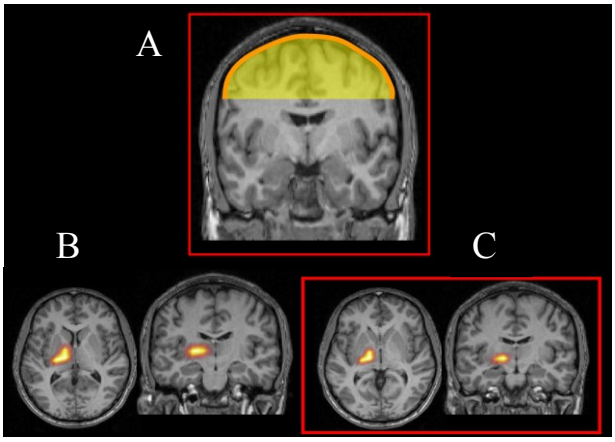

Figure 3. A. The yellow marked region shows the cortical areas which was considered as noise in the second run. B. Shows the results from the first run of the second simulation. C. Shows the results from the second run of the second simulation.

IV. Application to Parkinsonian DBS Patients

The DICS method was applied to 3 PD patients all of whom had deep brain stimulation electrodes on either side of the STN. The power spectrum showed clear peaks at the 90Hz stimulated frequency followed by its harmonics. In all the

patients the source for the stimulated frequency was found in the left-side of the brain as to be seen in the example of Fig. 4 in the slice plot with six slices of the brain. For this example patient the stimulation electrode on the left-side was stimulated and the right side was switched OFF. The locations for the stimulated frequency comprise the primary sensory motor cortex area, supplementary motor area (SMA), pre frontal cortex, STN, cerebellum and brain stem as shown in Fig. 4 on single slices for each source separately. The STN was correctly located by the applied source analysis method and the associated pathophysiological network with the STN was found.

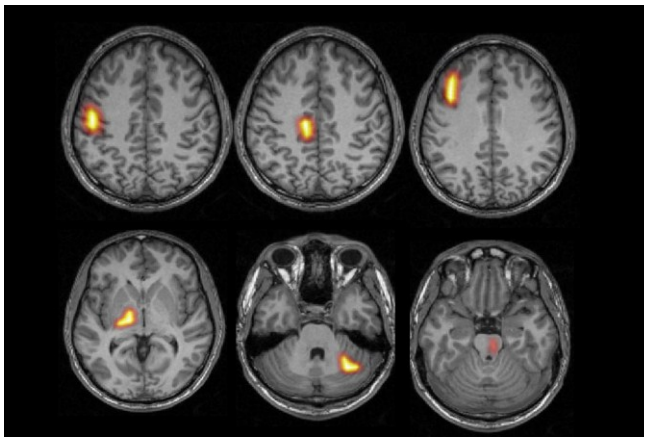

Figure 4. The single slice plots showing the network of sources for the stimulated frequency 90Hz in a Parkinsonian patient.

V. DISCUSSION

The first two aims of the studies in locating the STN-DBS electrode and identifying the network involved with STN were accomplished with the DICS algorithm. The first simulation gave some significant information about the location and need of the dipole orientation in the identified sources. The second simulation showed the first limitation of the method to identify the exact location of the sub-cortical STN-DBS source in the patients. The second limitation is application of the method to an artifact signal generated by the STN simulation in the scalp EEG. However, it is an important validation for the method because of the a-priori knowledge of the source which produces this artifact in the patients scalp EEG with DBS stimulation. The other frequency domain source analysis techniques like the sLORETA and synthetic aperture magnetometry (SAM) could be tested with the DICS algorithm to compare the localization accuracy of these methods in locating the STN-DBS electrode.

ACKNOWLEDGMENT

Support from the German Research Council (Deutsche Forschungsgemeinschaft, DFG, SFB 855, Project D2) is gratefully acknowledged.

REFERENCES

[1] G. Deuschl, et al., "Deep-brain stimulation for Parkinson's disease," *J Neurol*, vol. 249(suppl 3), pp. 36–39, 2002.

[2] G. Deuschl, R. Wenzelburger, F. Kopper, and J. Volkmann, "Deep-brain stimulation of the subthalamic nucleus for Parkinson's disease : a therapy approaching evidence-based standards," *J Neurol*, vol. 250(suppl 1), pp. 43–46, 2003.

[3] H. Stolze, et al., "Effects of bilateral subthalamic nucleus stimulation on parkinsonian gait," Neurology 67, pp. 144-146, 2001.

[4] S. H. Paek, J. H. Han, J. Y. Lee, C. Kim, B. S. Jeon, and D. G. Kim, "Electrode position determined by fused images of pre-operative and postoperative magnetic resonance imaging and surgical outcome after subthalamic nucleus stimulation," Neurosurgery 60, pp. 925-936, 2008.

[5] C. Pollo, et al, "Localization of electrodes in the subthalamic nucleus on magnetic resonance imaging," J Neurosurg 106, pp.36-44, 2007.

[6] T. S. Sumanaweera, J. R. Adler, S. Napel, and G. H. Glover, "Characterization of spatial distortion in magnetic resonance imaging and its implications for stereotactic surgery," Neurosurgery 35, pp.696-703, 1994.

[7] J. Y. Lee, et al., "Is MRI a reliable tool to locate the electrode after deep brain stimulation surgery? Comparison study of CT and MRI for the localization of electrodes after DBS," Acta Neurochir 152, pp.2029-2036, 2010.

[8] C. Hamani, J. A. Saint-Cyr, J. Fraser, M. Kaplitt, and A. M. Lozano, "The subthalamic nucleus in the context of movement disorders," Brain 127, pp. 4-20, 2004.

[9] T. E. Behrens, et al., "Non-invasive mapping of connections between human thalamus and cortex using diffusion imaging," Nat. Neurosci. 6, pp. 750-757, 2003.

[10] B. R. Aravamuthan, K. A. Muthusamy, J. F. Stein, T. Z. Aziz, and H. Johansen-Berg, "Topography of cortical and subcortical connections of the human pedunculopontine and subthalamic nuclei," Neuroimage 37, pp. 694-705, 2007.

[11] J. Gross et al., "Dynamic imaging of coherent sources: Studying neural interactions in the human brain" PNAS 98, pp. 694-699, 2001.

[12] M. Muthuraman et al., "Oscillating central motor networks in pathological tremors and voluntary movements. What makes the difference?" Neuroimage, in press 2012.

[13] M. Muthuraman, A. Galka, G. Deuschl, U. Heute, and J. Raethjen, "Dynamical correlation of non-stationary signals in time domain- A comparative study," Biomed. Sig Proc. Control 5(3), 205-213, 2010.

[14] D. B. Percival, and A. T. Walden, "Spectral analysis for physical applications: Multitaper and conventional univariate techniques," Cambridge: Cambridge univ. press, Chapter 7 pp. 331-374, 1993.

[15] D. Weinstein, L. Zhukov, and C. Johnson, "Lead-Field bases for electroencephalography source imaging," Anals of Biomed. Engg. 28, pp. 1059-1065, 2002.

[16] Z. Zhang "A fast method to compute surface potentials generated by dipoles within multilayer anisotropic spheres," Phys. Med. Biol. 40, pp. 335-349, 1995.

[17] J. C. de Munck "The potential distribution in a layered anisotropic spheroidal volume conductor," J. Appl. Phys. 64, pp. 464-470, 1990.

[18] Z. Zhang and D. L. Jewett "Insidious errors in dipole localization parameters at a single tim-point due to model misspecification of number of shells," Electroenceph. Clin. Neurophysiol. 88, pp. 1-11, 1993.

[19] M. Muthruaman, U. Heute, G. Deuschl and J. Raethjen "The central oscillatory network of the essential tremor," IEEE EMBC, pp.154-157, 2010.

[20] M.Muthuraman, J. Raethjen, H.Hellriegel, G. Deuschl and U. Heute "Imaging coherent sources of tremor related EEG activity in patients with Parkinson's disease," IEEE EMBC, pp.4716-4719, 2008.